Biomed Microdevices (2011) 13:683–693
DOI 10.1007/s10544-011-9538-2

A silicon-glass microwell platform for high-resolution imaging and high-content screening with single cell resolution

Thomas Wilhelm Frisk · Mohammad Ali Khorshidi · Karolin Guldevall · Bruno Vanherberghen · Björn Önfelt

Published online: 5 April 2011

Abstract We present a novel microwell array platform suited for various cell-imaging assays where single cell resolution is important. The platform consists of an exchangeable silicon-glass microchip for cell biological applications and a custom made holder that fits in conventional microscopes. The microchips presented here contain arrays of miniature wells, where the well sizes and layout have been designed for different applications, including single cell imaging, studies of cell-cell interactions or ultrasonic manipulation of cells. The device has been designed to be easy to use, to allow long-term assays (spanning several days) with read-outs based on high-resolution imaging or high-content screening. This study is focused on screening applications and an automatic cell counting protocol is described and evaluated. Finally, we have tested the device and automatic counting by studying the selective survival and clonal expansion of 721.221 B cells transfected to express HLA Cw6-GFP compared to untransfected 721.221 B cells when grown under antibiotic selection for 3 days. The device and automated analysis protocol make up the foundation for development of several novel cellular imaging assays.

Electronic supplementary material The online version of this article (doi:10.1007/s10544-011-9538-2) contains supplementary material, which is available to authorized users.

T. W. Frisk · B. Önfelt (✉)
Department of Microbiology, Tumor and Cell Biology, Karolinska Institutet,
Stockholm, Sweden
e-mail: bjorn.onfelt@ki.se

T. W. Frisk · M. A. Khorshidi · K. Guldevall · B. Vanherberghen · B. Önfelt
Cell Physics, Department of Applied Physics,
The Royal Institute of Technology,
Stockholm, Sweden

Keywords Single cell · Microwell · Automatic image analysis · Screening · Fluorescence imaging · Clonal expansion

1 Introduction

The importance of single cell analysis is becoming increasingly apparent in cell biology (Spudich and Koshland 1976; Templer and Ces 2008). As cell populations are inherently heterogeneous, individual cells respond differently to various drugs or treatments and, for example, a few cells escaping treatment could be important for the progression of cancer. Heterogeneity within the immune system is well documented. Each T cell carries an antigen-specific T cell receptor which, upon sufficient stimulation (e.g. by a virus infection), can undergo activation and clonal expansion. This means that the T cell repertoire has to be broadly heterogeneous in its TCR specificity to be able to respond to the multitude of viruses or cell transformations that can occur. Similarly, an individual's repertoire of natural killer (NK) cells is heterogeneous in terms of the numbers of activating and inhibitory receptors expressed as well as their qualitative and quantitative response to viruses and tumors (Höglund and Brodin 2010)

In order to resolve cell population heterogeneity it has been suggested that approximately 1,000–10,000 individual cells need to be analyzed (Givan 2001; Svahn and van den Berg 2007). Thus, high-throughput experimental approaches are required to address cellular heterogeneity in many biological questions. Recent progress in the fields of microfabrication, microscopy and computing have paved the way for more efficient tools for studies of time resolved live cell imaging at the single cell level. For example, with

cells confined in separated compartment or wells on large arrays quantitative data can be collected, yielding more information of cell-to-cell variations and accurate statistics to resolve the heterogeneity of cell populations.

Many devices for single cells studies have been described. Some are based on sedimentation of cells into wells (Revzin et al. 2003; Chin et al. 2004; Dusseiller et al. 2005; Rettig and Folch 2005; Revzin et al. 2005; Yamamura et al. 2005; Deutsch et al. 2006a, b; Guldevall et al. 2010), others trap cells using flow systems (Carlo and Lee 2006; Tan and Takeuchi 2007; Skelley et al. 2009), some use suction immobilization (Lehnert et al. 2002; Liu and Sun 2009; Schiffenbauer et al. 2009) or use microengraving, where cells are trapped between cover-glass and wells formed in polydimthylsiloxane (PDMS) (Love et al. 2006; Han et al. 2010). Surface modification techniques aimed at single-cell immobilization and improved biocompatibility have also been applied (Suh et al. 2004; Mohr et al. 2006; Moeller et al. 2008). Microdevices trapping cells in wells for analysis of single cells, clonal expansion or cell-cell interactions have also been described (Schiffenbauer and Israeli 2007; Lindstrom et al. 2008). Yet another trapping method is the droplet microfluidics where cells are contained in picoliter two-phase systems (He et al. 2005). However, few of these devices allow long-terms survival of cells, high resolution imaging or have a relatively low density of compartments making them unsuitable for high throughput assays.

In this study we present a platform for high-resolution imaging and screening aimed at biological assays where it is important to study large number of cells at the single cell level. To make a device that would be useful on a daily basis in a biological lab we have prioritized the following criteria: 1. the device should be compatible with high-throughput automatic microscopic readout and analysis, 2. the device should be biocompatible allowing long term assays, and, 3. the device should be easy to use. Our device is based on silicon-glass microchips with varying number of square wells depending on the application (Fig. 1, Table 1). The microchips are easily integrated with a custom made holder that fits on most microscopes, making it suitable for various cell assays with microscopic readout and automated analysis.

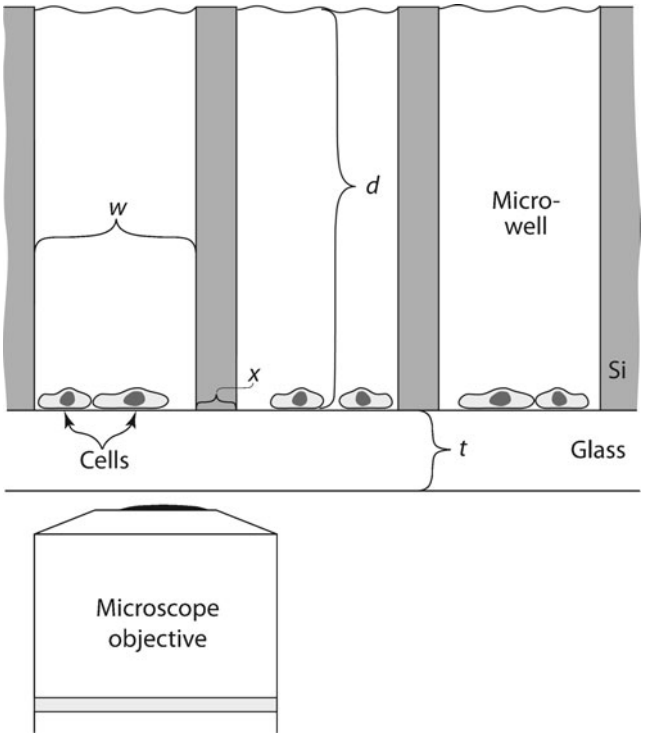

Fig. 1 Schematic picture showing a cross-section of the microchip. All chips were made from silicon (Si) wafers with a thickness (*d*) of 300 or 500 μm, bonded to glass with a thickness (*t*) of 175 μm allowing imaging with an inverted microscope. The well width (*w*) and wall width (*x*) was varied for the different designs. The sketch is not to scale

2 Methods

2.1 Fabrication of silicon-glass microwell chip

The fabrication process is sketched in Fig. 2. Initially, 100 mm silicon wafers, 300 μm thick, were cleaned and wet oxidized at 1,100°C in hydrogen and oxygen to 1–2 μm oxide thickness. The oxide has dual purposes, forming both a good masking material for the deep well etch, as well as a backside etch stop during the final phase of the deep etch. A positive thick photo resist AZ 9260 (MicroChemicals GmbH, Ulm, Germany) was spun on to the wafer at 1,500 rpm for 30 s. After soft bake at 90°C for 600 s and re-hydration for 45 min in ambient atmosphere, the mask exposure was performed in multi exposure mode (4×2.5 s) in a Mask Aligner (MicroTec MA/BA6, SÜSS MicroTec Lithography GmbH, Garching, Germany). Baking was performed in a step-wise fashion: ramping from 90°C to 120°C with duration of 1 h per 10°C. The oxide pattern was then etched dry (15 sccm CHF_3, 5 sccm CF_4, 50 sccm Ar at 350 W) for 7 min in a dry oxide etcher (Precision 5000 Mark II, Applied Materials, Austin, Texas, USA). The silicon wells were then deep etched (DRIE: SF_6 and C_4F_8 alternating Bosch process) during 120 min in a dry ion plasma etcher (STS ICP, Surface Technology Systems, Newport, UK). Figure 3 shows representative scanning electron microscopy (SEM) images validating the etching protocol. Microchips that were diced across the wells and imaged by SEM showed that the well shapes were conserved throughout the depth of the microchips (data not shown).

Following cleaning in oxygen plasma (500 sccm, 1,000 W) during 30 min, oxide strip (concentrated HF) and wet clean (7-UP; H_2SO_4 and H_2O_2, 3:1, at 130°C), the wafers were again furnace wet-oxidized to an approximate surface oxide

Table 1 Dimensions, parameters and applications for the different microchips produced

Design no	Well width, w (μm)	Wall thickness, x (μm)	No of wells	Application
1	30	20	90 000–102 400	Screening/imaging cell-cell interactions (Guldevall et al. 2010)
2	50	30	32 400–40 000	
3	300	100	100–600	Ultrasonic manipulation (Vanherberghen et al. 2010)
4	450	350	400	Long-term imaging of small cell populations (Khorshidi et al. 2011)
5	700	100	400	

thickness of 200 nm, in order to increase the biocompatibility (Stensaas and Stensaas 1978; Voskerician et al. 2003) and enabling cleaning and re-useage of the chips. A brief pre-treatment step was carried out through dipping the wafers in 7-UP, rinsing in deionized water and drying in hot hydrogen. Finally, 175 μm thick borofloat glass (Compart Tech, UK) was anodically bonded to the silicon wafer (−600 V at 420°C for 15 min). The wafers were then diced with a standard diamond blade at 30 krpm (0.5 mm/s feed rate) into chips with a 22×22 mm footprint, thus fitting in 30 mm petri dishes and compatible with microscope glass slide holders.

2.2 Electron microscopy

Uniformity of the masking and etching fabrication processes were evaluated with SEM (Ultra 55, Zeiss, Germany) at various degrees of magnification (Fig. 3). In order to avoid charge build-up problems, the filament voltage was kept low (0.3–1 kV) at all scans.

2.3 Chip holder

A few holder designs were manufactured and tested. We found that a three piece design with a circular base plate proved particularly functional (Fig. 4). It consists of a bottom holder made in titanium or polyether ether ketone (PEEK) with a 0.2 mm thin flange, enabling high resolution imaging with an inverted microscope. The top lid, made in the transparent material poly-methyl methacrylate (PMMA) clamps a polydimethyl siloxane (PDMS, Sylgard 184, GA Lindberg AB, Sweden) gasket to the silicon chip, thus forming an open liquid reservoir over the microchip. The lid has a 20×20 mm hole in the center, creating an open system allowing addition of material, e.g. cell culture medium, fluorescent probes or drugs, to the cells. The bottom holder and the lid were clamped together with four neodymium magnets (Nd-35, diameter 3 mm, length 6 mm), embedded in the top piece positioned 200 μm above four magnetic stainless steel discs embedded in the base plate, enabling a tight seal. The liquid volume above the chip can be as large as 2.5–3 ml, providing an abundant supply of nutrients to the cells, as well as a buffering reservoir for metabolite products. A lid from a standard 30 mm PE petri dish prevented both liquid evaporation and contamination.

2.4 Cells

The untransfected human B cell line 721.221 (referred to as 221) and the stable transfectant 221/Cw6-GFP have been previously described (Shimizu and Demars 1989; Davis et al. 1999). Both were grown in RPMI 1640 medium (Sigma) supplemented with 10% FCS, 2 mM L-glutamine, 1 × non-essential amino acids, 1 mM sodium pyruvate, 50 units/ml penicillin-streptomycin, and 50 μM β-mercaptoethanol. 221/Cw6-GFP was grown under antibiotic selection (1 mg/ml G418 Geneticin) to maintain stable expression of Cw6-GFP.

2.5 Labeling

For labeling, cells were centrifuged at 300g to pellet cells and subsequently stained in 37°C RPMI 1640 with 10 μM Far Red DDAO-SE (Far Red) or 0.5 μM Calcein AM (both from Invitrogen, Carlsbad, CA, USA) for 15 min at 37°C, 5% CO_2. After staining, cells were washed twice in RPMI-1640 and re-suspended in the cell culture medium described above.

2.6 Seeding cells in the device

Loading of cells in the microchip was similar to what has been described previously (Guldevall et al. 2010). Briefly, after sterilization and priming, the chip was placed in the holder and 30 000–50 000 cells, suspended in 1 ml cell culture medium, were added. The cells were left to sediment by gravity to the bottom of the wells, the chip washed to remove cells outside of the wells, and more medium (1–2 ml) added.

2.7 Flow cytometry

Mixtures of dye-labeled cells were analyzed by flow cytometry (BD FACS Calibur) using FL-1 for detection of Calcein and FL-4 for detection of Far Red.

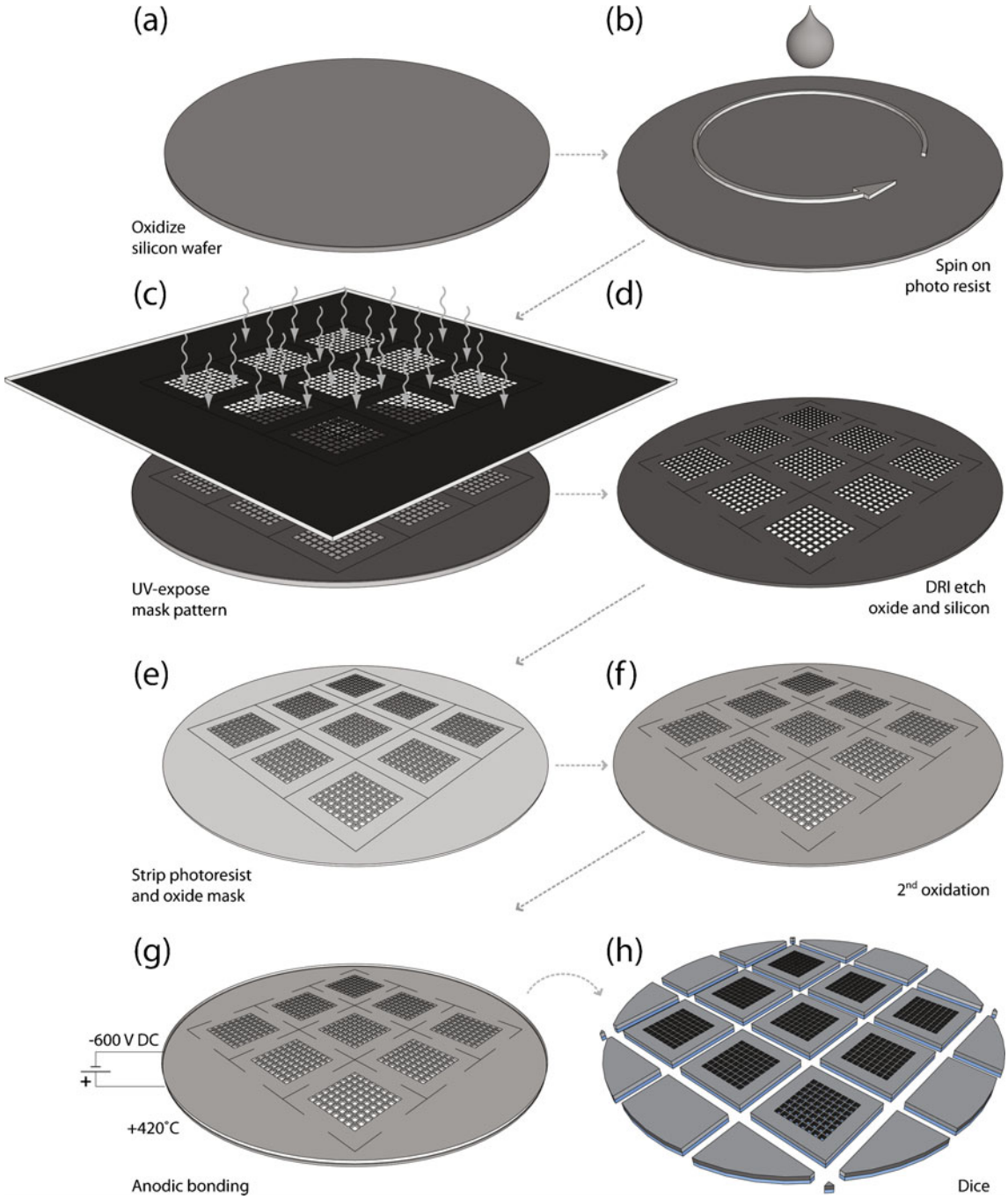

Fig. 2 Schematic outline of the microchip fabrication process. (**a**) Oxidized silicon wafer. (**b**) Spin coating of wafer with photoresist. (**c**) Masked UV-exposure of photosensitive resist layer. (**d**) Plasma etching of the oxide and silicon. (**e**) Removing photoresist and oxide mask. (**f**) Oxidation of the wafer after the strip of the masking photoresist. (**g**) The anodic bonding of the glass bottom to the silicon 'grid'. (**h**) Dicing to individual chips

2.8 Optical microscopy and screening

Imaging was performed with an inverted laser scanning confocal microscope (LSM 5 Pascal, Carl Zeiss, Oberkochen, Germany) equipped with a motorized stage. For screening applications a 10× 0.3 NA objective and an opened pinhole were used (Fig. 4) The dichroic beam-splitter HFT488/543/633 was used for all fluorescence microscopy, and the individual imaging set up (excitation/filter) for the different fluorescent probes was as follows: Calcein (488 nm/BP505-530) and Far Red (633 nm/LP650). Both bright field images and fluorescent images were acquired

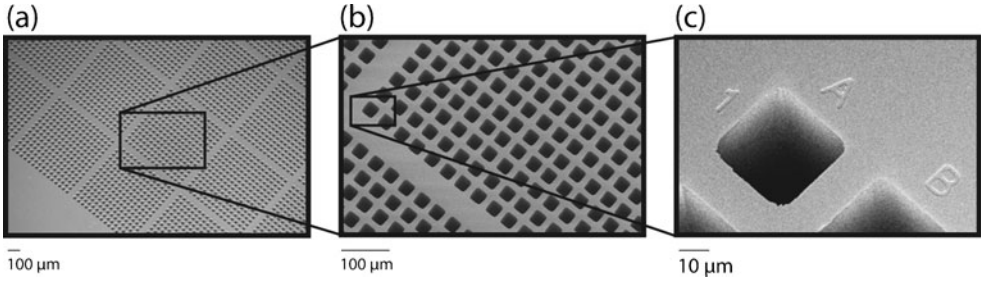

Fig. 3 Characterization of the microchips by SEM (**a**)–(**c**). Sections of a microwell chip containing 30×30 µm wells arranged in 20×20 sections each containing 15×15 wells imaged at 100× (**a**), 400× (**b**) and 4,500× (**c**). In (**c**) the row and column indices etched in the silicon surface can be seen

and saved for analysis. For screening applications (using a well-size of 50×50 µm), microchips where the wells were distributed in 20×20 groups of 9×9 wells were used (totally 32 400 wells). Images (1024×1024 pixels at eight bit) were acquired of each group of 81 wells using a 10× objective and the images were saved in a database for further processing. This layout of the chip made it possible to image defined groups of 9×9 wells and facilitated accurate image analysis of individual images rather than on large mosaic images where all images had been stitched together. This was particularly important when the same chip was analyzed on separate occasions since it made it easy to relocate and evaluate the content of specific wells.

2.9 Automatic counting of cells

For automatic analysis of the screening results and quantification of the number of cells in each well a home-developed routine in Matlab (The MathWorks, Inc., Natick, MA, USA) was used. The steps followed by the program are shown as a flowchart in Fig. 5 and explained in the sections below.

2.9.1 Identification of wells

Binary images, obtained by applying a threshold to the bright-field images, were used for segmenting individual wells from background. The coordinates of the top left corner of each well in the image frame were recorded and the corresponding

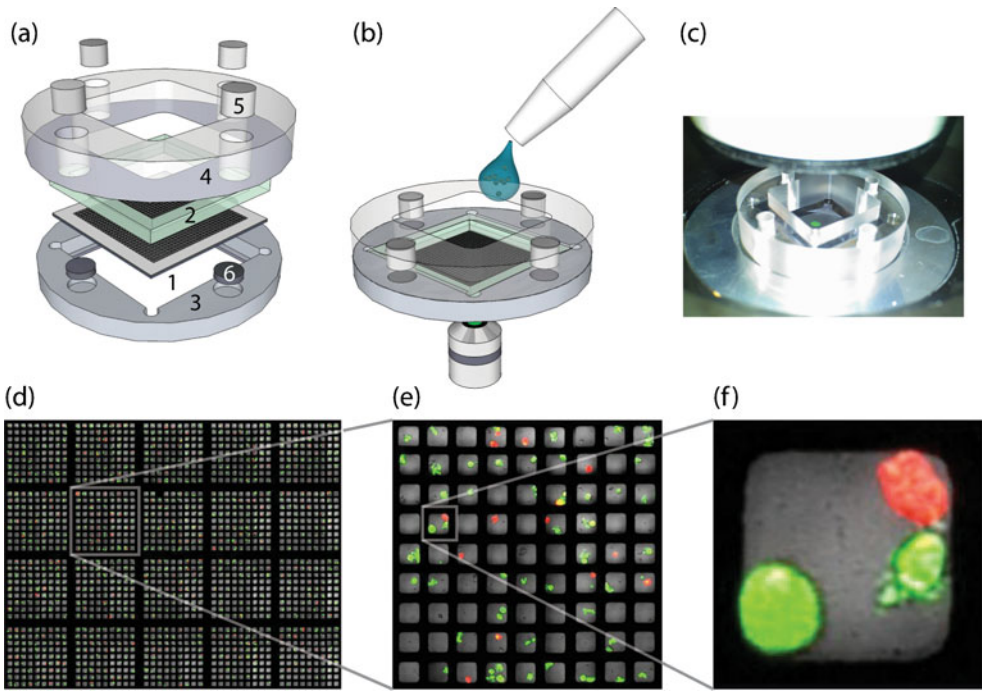

Fig. 4 Design, assembly and applications of the microchip device. (**a**) Schematic picture showing an exploded view of the device. The microchip (*1*) and gasket (*2*) were sandwiched between bottom (*3*) and top (*4*) parts of the holder, which were held tightly together by neodymium magnets (*5*) attracted to stainless steel cylinders (*6*). (**b**) With an open device, cells could easily be loaded into the microwells from the top and imaged in an inverted microscope. (**c**) Photograph of the assembled holder placed in an inverted microscope. (**d**)–(**f**) Sections of a larger tile scan showing overlaid bright field and fluorescence images of 221 B cells double labeled with Calcein (*green*) and Far Red (*red*) imaged in 50×50 µm wells with a 10x objective. Dead cells are seen as only red. (**d**) A section of 5×4 individual images. (**e**) An individual image showing the 9×9 wells containing a mixture of red and green cells. (**f**) Content of a single well with two live and one dead cell

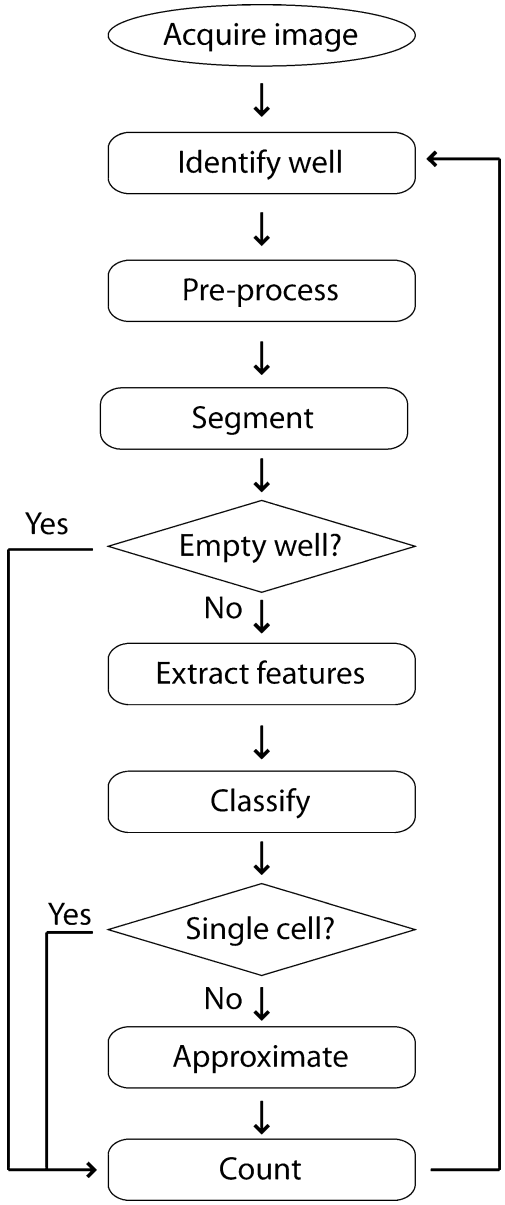

Fig. 5 Flow chart demonstrating the sequence of steps in the automatic cell counting program. Firstly, the program discriminated between empty and non-empty wells. In non-empty wells individual objects were classified as single cells or clusters, followed by assessment of the number of cells in the clusters and counting. The process was repeated until all wells were analyzed

fluorescence images were cropped into smaller sections (70× 70 μm) so that the interior of each well was covered. Each section was numbered giving each well an identity, so that they could easily be relocated in the original images.

2.9.2 Pre-processing

Before cropping the fluorescence images, a Gaussian kernel filter was applied to reduce noise. Then, the fluorescence images were multiplied by the corresponding binary image of the wells to subtract undesirable regions of background, e.g. auto-fluorescence from the silicon.

2.9.3 Segmentation

Otsu's method was used to separate fluorescent objects (cells) from background. This method is based on finding the optimum threshold to separate two classes of pixels (foreground and background) that minimizes the weighted within-class variance (this is the same as maximizing the between-class variance) (Otsu 1979). The objects detected by this method were visually assessed and divided into two classes; singles or clusters.

2.9.4 Feature extraction

To be able to separate single cells from clusters of cells, some descriptive features based on pixel values and spatial arrangement within the objects were extracted. These features were intensity, area, perimeter and compactness, where the compactness was defined as

$$\text{Compactness} = \frac{\text{Perimeter}^2}{4\pi \times \text{Area}}$$

2.9.5 Classification

Analysis showed that intrinsic variations of the fluorescence intensity between the individual cells were too large to use this parameter for classifying the objects as single cells or clusters. However, the morphometric parameters area, perimeter and compactness could be used for classification (Fig. 6(a)–(c)).

Briefly, each object can be represented by its n descriptive features as a vector x in the n dimensional feature space, $\mathscr{R}^n$. Then, it is possible to use a discriminate rule to divide $\mathscr{R}^n$ into C separate regions $R_1,\ldots, R_C$ ($\cup R_i=\mathscr{R}^n$ and $i=1,\ldots,C$). Suppose data come from C classes, where each class c_i has a probability density function in $\mathscr{R}^n$. The discriminate rule allocates each test point x_t to c_i if $x_t \in R_i$. In our application, there were three features ($n=3$) and two classes of data (single cells and clusters, $C=2$). Since visual assessment showed that the number of single cells was far greater than the number of clusters, we assumed one class of objects (single cells) as our data base. This data base had a Gaussian distribution with a covariance matrix Σ and a mean value μ, and the Mahalanobis distance (Fraser et al. 2003) could be obtained as

$$\Delta = \left[(x_t-\mu)^T \sum{}^{-1} (x_t-\mu)\right]^{\frac{1}{2}}.$$

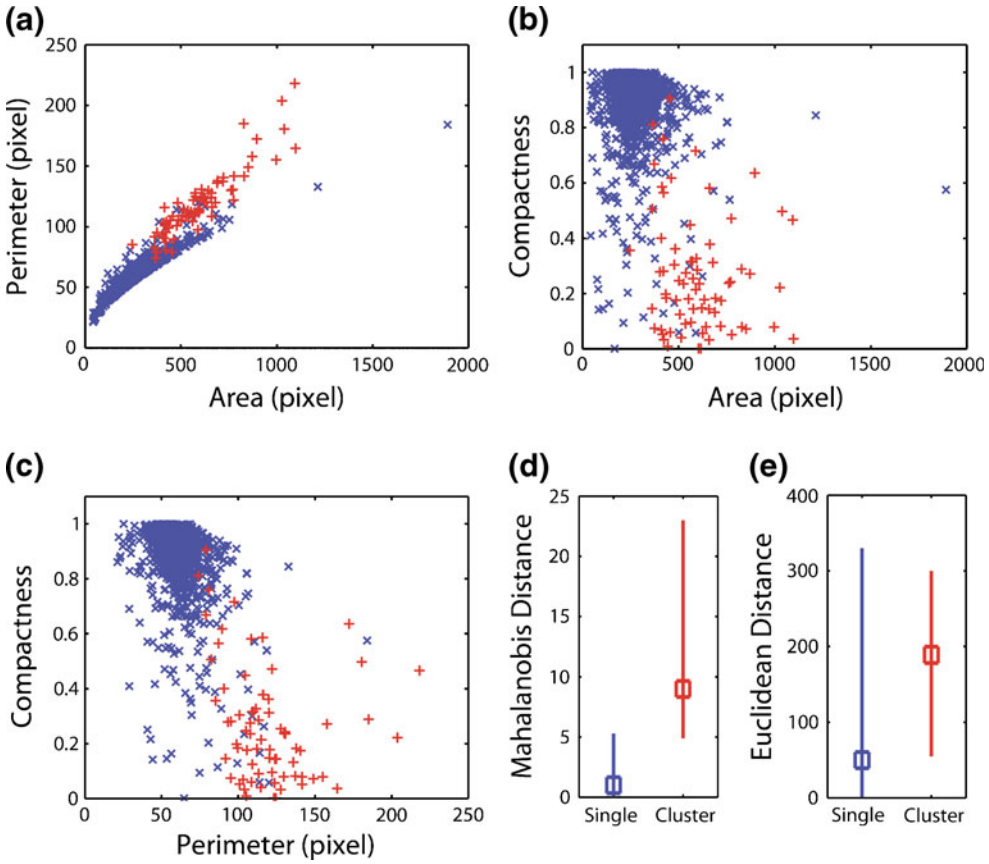

Fig. 6 Comparison of morphometric features used for classification of objects into single cells or clusters. (**a**)–(**c**). Objects were visually assessed as single cells (*blue* 'x') or clusters (*red* '+'). (**a**) Perimeter plotted versus area. (**b**) Compactness plotted versus area. (**c**) Compactness plotted versus perimeter. (**d**) The Mahalanobis distance measurements for single cells and clusters. (**e**) The Euclidean distance measurements for single cells and clusters

Based on the training data set (manually analyzed objects), unbiased estimates of Σ and μ were sample covariance matrix S and sample mean $\bar{x}$, respectively. Then, estimated Mahalanobis distance of each test point from sample mean of training data set could be written as

$$d_M = \left[(x_t - \bar{x})^T S^{-1} (x_t - \bar{x})\right]^{\frac{1}{2}}.$$

The value of d_M was measured for all test points and used to classify the objects as either inside or outside the base class (single cells). If the distance of x_t was greater than a predetermined threshold this test point would be regarded as a cluster, otherwise it belongs to the single cell class.

For validation of the classifier performance, the leave-one-out method was used. Hence, for testing each sample, one data point (the one left out) in the base space was used to calculate the distance in the base space group. The validation results are presented in the form of bars indicating the maximum and minimum of Mahalanobis distance and it is compared to the Euclidean distance when the covariance matrix is equal to identity matrix ($\Sigma = I$) (Fig. 6(d)–(e)). Evaluation of the classifier showed that the accuracy of the classifier is about 98% (further explained in the Supporting information).

2.9.6 Approximation and counting

Once the objects were classified as single cells or clusters, we approximated the number of cells in each cluster based on area; the area of the clusters was divided by the average area of a single cell. Finally, the number of cells in each well was counted.

3 Results

3.1 Assessing the automatic cell counting accuracy

To test the accuracy of our automated counting method we compared its performance to manual counting of cells distributed in the micro-well chips. Human B cells (221 cell line) labeled with either Calcein or Far Red were seeded into two different microchips and part of the chips were screened and the number of cells within each well was scored automatically and manually. Figure 7 shows representative images of Calcein and Far Red stained cells inside microwells. Overall, we found only small discrepancies between the two methods. The success rates for automatic detection of the total number of cells were 99.7% (n=905) and 97.4% (n=1,395) for Calcein and Far Red labeled cells,

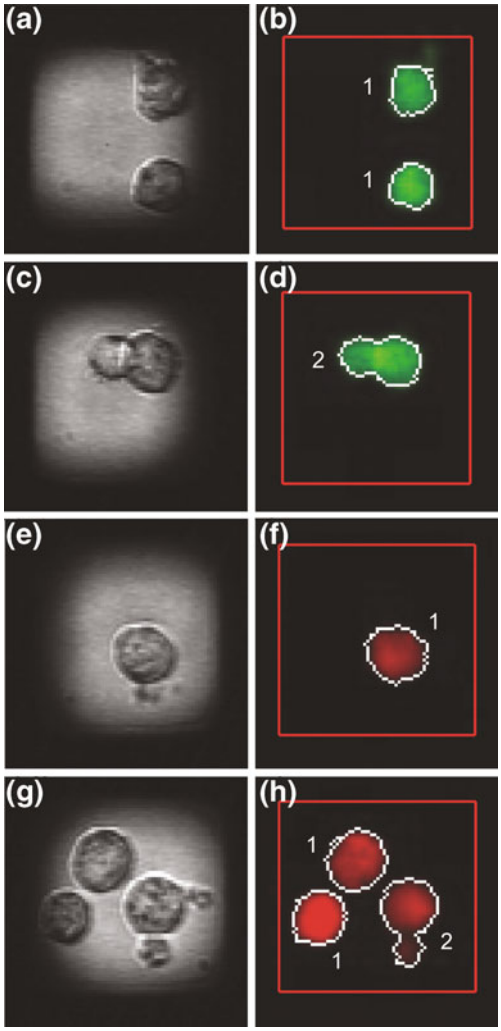

Fig. 7 Automatic detection and counting of cells in individual wells. (**a**)–(**d**) Bright field (**a**, **c**) and fluorescent (**b**, **d**) images of wells containing 221 cells stained with Calcein showing examples of separated single cells (**a**, **b**) and cluster of cells (**c**, **d**). (**e**)–(**h**) Bright field (**e**, **g**) and fluorescent (**f**, **h**) images of wells containing 221 cells stained with Far Red showing examples of a single cell (**e**, **f**), a cluster of cells as well as single cells (**g**, **h**). The red lines in the fluorescence images outline the section that was cropped (70× 70 μm) and analyzed. The white lines outline the detected objects and the white numbers indicate the number of cells scored in each object

respectively. When looking at the distributions of cells per well it was evident that the discrepancy between the two methods increased the more cells were in the wells (Table 2). This likely reflects that our program, although good at distinguishing single cells from clusters, was not as good at counting the number of cells inside clusters compared to the human eye. Furthermore, the correlation between the two methods was better for cells stained with Calcein than for cells stained with Far Red. This is most likely correlated with a more homogeneous intracellular staining found for Calcein leading to a higher accuracy of segmentation and determination of the morphometric parameters.

As a next step we wanted to know whether our automatic counting method could allow accurate determination of frequencies of differently labeled cells inside the microchip based on fluorescence. To test this, we mixed cells labeled with either Calcein or Far Red at four different frequencies. We then used our program to count the total number of green and red cells and determined their frequencies within the total population. When comparing our results to flow cytometry, we found comparable ratios of cells using the two methods (Table 3). Thus, these data showed that our screening platform and automatic image analysis is suitable for applications where mixtures of differently labeled cells are used.

3.2 Clonal expansion in the microwell platform

Finally, we wanted to determine whether the microdevice could be used for selective survival and expansion of individual cells over extended periods of time. To test this we mixed two cell types, a wild-type 221 cell line and the same 221 cell line transfected to stably express HLA-Cw6-GFP (221/Cw6-GFP) under a G418 antibiotic selection marker. When cultured in the presence of G418, the non-fluorescent 221 cells should die while the resistant fluorescent 221/Cw6-GFP should survive and proliferate. The cell mixture was distributed on the microwell array, allowed to sediment completely and imaged with bright-field and fluorescence detection. Based on manual inspection of the bright field images it was determined which wells contained cells and which were empty, and by automatic counting of the fluorescence image it was determined which wells that contained fluorescent cells (221/Cw6-GFP). After 3 days of culture in the presence of antibiotic selection, the microwell array was screened again in the same manner and by manual inspection of the bright field image it was determined which wells contained live cells and which contained dead cells. Importantly, this assessment was done without looking at the fluorescence image. Instead, detection of the wells containing fluorescent cells was again done using the automatic counting program. Figure 8 shows a summary of the results.

In total the content of 3,742 wells was assessed and on day 1 1,460 wells were scored as empty and 2,282 wells as non-empty (Fig. 8(a)). Out of the non-empty wells, 322 wells contained fluorescent cells. Figure 8(b) shows the content on day 3 from the 1,460 wells that had been scored as empty day 1. The vast majority of these wells remained empty (n=1,331), while some wells containing dead (n=111) and live (n=18) cells were also found. This could be because some cells sedimented slowly and reached the well bottom after the screening on day 1, or cells could migrate

Table 2 Accuracy of automatic compared to manual counting. Calcein or Far Red labeled cells were distributed in the wells and the number of cells in each well was counted manually or automatically. The manual counting represents 100% and *n* refers to the number of wells counted for each condition

Number of cells per well	0	1	2	3	4
Calcein labeled cells	100% (*n*=2,011)	99.9% (*n*=707)	99.4% (*n*=175)	95.8% (*n*=23)	–
Far Red labeled cells	100% (*n*=1,519)	98.7% (*n*=999)	98.7% (*n*=315)	94.9% (*n*=68)	94.8% (*n*=13)

between wells during the long incubation time. The fact that more wells containing dead cells were scored is consistent with our observation that dead cells were more prone to detach from the well bottom and drift away. Figure 8(c) shows the content on day 3 from the 1960 wells that had been scored as non-empty and non-fluorescent on day 1. About 92% of these wells were now scored as being empty or containing dead cells (*n*=1,795), while the rest were determined to contain live cells (*n*=165). Figure 8(d) shows the content on day 3 from the 322 wells that had been scored as non-empty and fluorescent day 1. A majority (95%) of these wells are still scored as containing live and fluorescent cells (*n*=305). If this data is summarized, the non-fluorescent cells were much more likely to die during the incubation with G418 compared to the fluorescent cells (92% vs 5%, see example in Fig. 8(e)). Furthermore, in several of the wells containing live and fluorescent cells day 3 we observed significant increase in the number of cells compared to day 1 (Figs. 8(f) and (g)). Representative images from this experiment can be found as movies in the supporting information (ESI movie). Taken together, this data shows that our microwell platform is suitable for studies of cell survival and clonal expansion, e.g. to detect resistance to drugs (Lindstrom et al. 2008) or T cell activation after stimulation with antigen.

4 Discussion

We here present a versatile device suitable for a range of applications, e.g. screening large numbers of cells with single cell resolution or interactions between individual cells (Guldevall et al. 2010) or small populations (Khorshidi et al. 2011) of immune cells and target cells. Parameters such as well size, distribution and wall thickness were optimized for the specific experimental applications in mind. Up till now we have fabricated five different designs with varying well sizes (30–700 μm) and wall thickness (20–350 μm) yielding chips with the number of wells ranging from 100 to 102,400 (Table 1).

This study was focused on a microchip optimized for screening and high-resolution imaging of single or a few cells located inside smaller silicon wells (30–50 μm). The microchips were made compatible with high-resolution imaging by bonding a thin glass (175 μm) to the chip, and with high-content screening by designing a layout where the wells were arranged in 400 (20×20) sections of 9×9 wells over the chip. Each 9×9 section could be scanned separately in a single image with a 10× objective consequently allowing all 400 sections to be scanned and saved as individual files. This facilitated the process of locating specific wells when chips were screened several times as well as the automated analysis since it could be done on individual images, rather than reconstructed tiles scans.

In the fabrication process, a first oxidation step rendered a secondary masking layer, which was beneficial when etching through the silicon wafer, since it ensured that the mask (and thus the well walls) integrity was kept even if the layer of photoresist was consumed in peripheral areas. The second oxidation of the wells interior walls (as well as the top and bottom wafer surfaces) yielded a tough silicon dioxide layer, increasing the biocompatibility of the chip and enabling harsh washing protocols, thus enabling re-use of the chips.

To enable high-throughput screening with detection of single cells in a device containing 32 400–102 400 microwells, an automated image analysis program to count the number of cells within each well was developed. The

Table 3 Comparison between counting by FACS and automatic counting. Calcein or Far Red labeled cell were mixed in the microchip at different frequencies and counted automatically using our program or by FACS. The top row of the table indicates the intended frequencies of Calcein (G) or Far Red (R) labeled cells

Percentage of cells	0G[a]–100R[b]	30G–70R	50G–50R	100G–0R
FACS counting (*n*=10,000)	0.8%–98.2%	33.3%–65.9%	49.3%–49.6%	98.4%–0.7%
Automatic counting	0%–100% (*n*=1,841)	32.8%–67.2% (*n*=420, *n*=859)	47.8%–52.2% (*n*=867, *n*=946)	100%–0% (*n*=1,126)

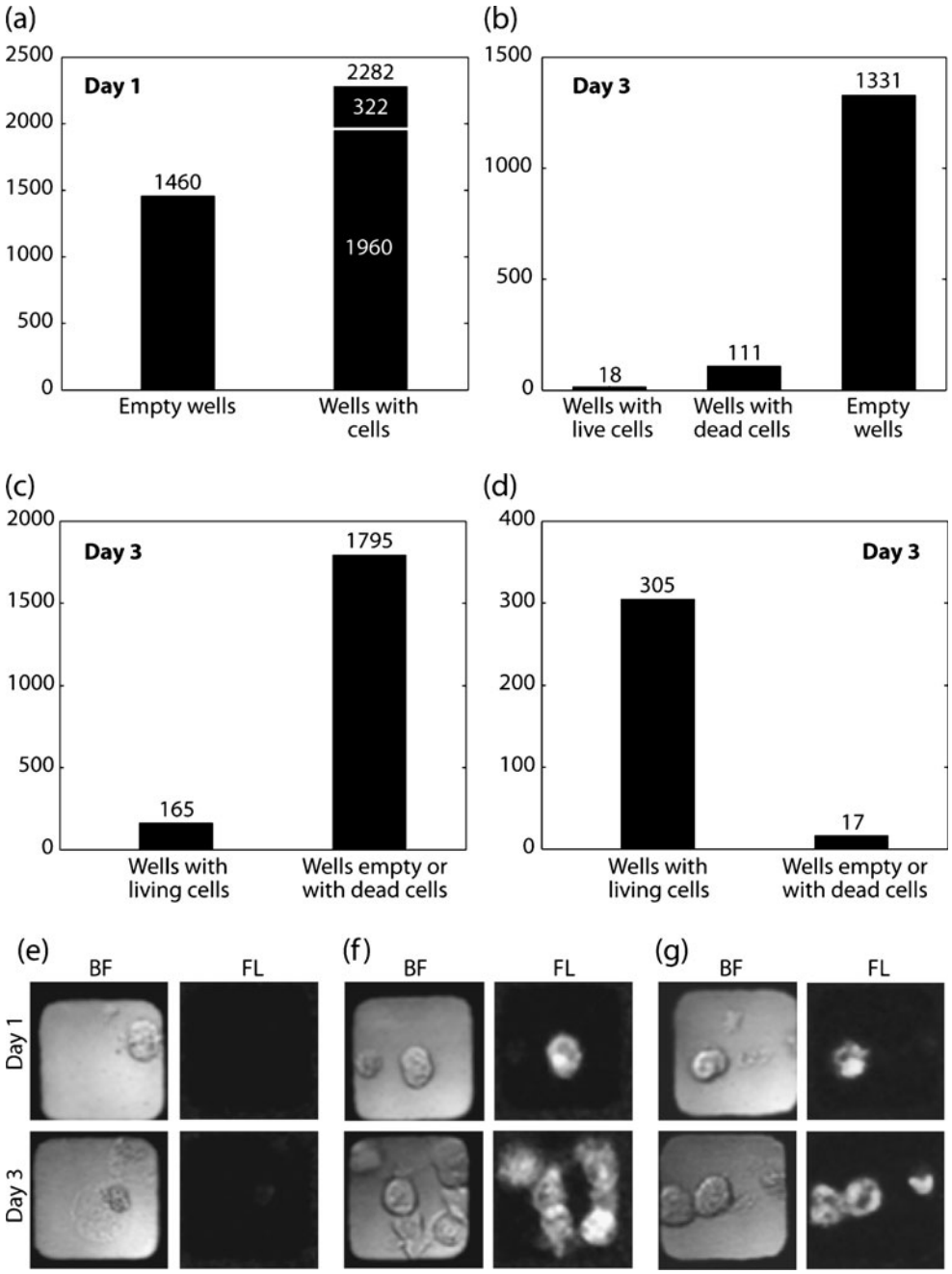

Fig. 8 Clonal expansion in the microwell platform. (**a**) Histogram showing wells scored as empty and non-empty on day 1. Out of the non-empty wells 322 contained fluorescent cells. (**b**) Histogram showing day 3 screening results from the wells that had been scored as empty on day 1. (**c**) Histogram showing day 3 screening results from the wells that had been scored as containing non-fluorescent cells on day 1. (**d**) Histogram showing the day 3 screening results from the wells that had been scored as containing fluorescent cells on day 1. (**e**)–(**g**) Representative bright field (BF) and fluorescence (FL) images of individual wells imaged on day 1 (upper row) and day 3 (lower row). (**e**) A single non-fluorescent cell that died between day 1 and day 3. (**f**)–(**g**) Single fluorescent cells that proliferated between day 1 and day 3

software could efficiently distinguish single cells from clusters of cells, but assessing the number of individual cells making up the clusters proved to be more challenging. As a consequence, the more cells that were in individual wells the less precise the counting was. The accuracy of counting was also dependent on the fluorescent dyes used; a more homogeneous intracellular distribution of the fluorescence gave better results. Overall, the developed software proved to have a satisfactory accuracy and speed for most applications but our studies show that the labeling and imaging conditions should be optimized for the best results.

The long-term survival of cells in this device together with the low frequency of cells migrating between wells (Guldevall et al. 2010) makes it possible to design experiments spanning several days. To illustrate this we studied clonal expansion of cells against an antibiotic selection where the content of each well was scored twice, 3 days apart. This new device combined with automatic counting makes it possible to efficiently study many cellular processes at the single cell level. This is likely to lead to new knowledge about many different cell types, not least NK cells, where the implications of cell-to-cell variations are becoming increasingly apparent.

Acknowledgements We are grateful for financial support from KTH Future Faculty, the Swedish Foundation for Strategic Research (SSF), personal and collaboration grants from the Swedish Research Council (VR), the Göran Gustafsson Foundation and the Harald Jeansson Foundation. We would also like to thank Rolf Helg for helping out in the fabrication of the chip holder, and Agneta Önfelt for help with manual counting of cells.

References

D.D. Carlo, L. Lee, Anal. Chem. **78**(23), 7918–7925 (2006)
V.I. Chin, P. Taupin, S. Sanga, J. Scheel, F.H. Gage, S.N. Bhatia, Biotechnol. Bioeng. **88**(3), 399–415 (2004)
D.M. Davis, I. Chiu, M. Fassett, G.B. Cohen, O. Mandelboim, J.L. Strominger, Proc. Natl. Acad. Sci. U. S. A. **96**(26), 15062–15067 (1999)
A. Deutsch, N. Zurgil, I. Hurevich, Y. Shafran, E. Afrimzon, P. Lebovich, M. Deutsch, Biomed. Microdevices **8**(4), 361–374 (2006a)
M. Deutsch, A. Deutsch, O. Shirihai, I. Hurevich, E. Afrimzon, Y. Shafran, N. Zurgil, Lab. On. Chip. **6**(8), 995–1000 (2006b)
M.R. Dusseiller, D. Schlaepfer, M. Koch, R. Kroschewski, M. Textor, Biomaterials **26**(29), 5917–5925 (2005)
A.M. Fraser, N.W. Hengartner, K.R. Vixie, B.E. Wohlberg, Neural Networks, Neural Network International Joint Conference (2003)
A.L. Givan, Meth. Cell Biol. **63**, 19–50 (2001)
K. Guldevall, B. Vanherberghen, T. Frisk, J. Hurtig, A. Christakou, O. Manneberg, S. Lindstrom, H. Andersson Svahn, M. Wiklund, B. Onfelt, PLoS ONE 5(11) (2010).
Q. Han, E.M. Bradshaw, B. Nilsson, D.A. Hafler, J.C. Love, Lab. On. Chip. **10**(11), 1391–1400 (2010)
M.Y. He, J.S. Edgar, G.D.M. Jeffries, R.M. Lorenz, J.P. Shelby, D.T. Chiu, Anal. Chem. **77**(6), 1539–1544 (2005)
P. Höglund, P. Brodin, Nat. Rev. Immunol. **10**(10), 724–734 (2010)
M.A. Khorshidi, B. Vanherberghen, J. Kowalewski, K.R. Garrod, S. Lindström, H. Andersson-Svahn, H. Brismar, M.D. Cahalan, B. Önfelt, submitted, (2011)
T. Lehnert, M.A.M. Gijs, R. Netzer, U. Bischoff, Appl. Phys. Lett. **81** (26), 5063–5065 (2002)
S. Lindstrom, R. Larsson, H.A. Svahn, Electrophoresis **29**(6), 1219–1227 (2008)
X.Y. Liu, Y. Sun, Biomed. Microdevices **11**(6), 1169–1174 (2009)
J.C. Love, J.L. Ronan, G.M. Grotenbreg, A.G. van der Veen, H.L. Ploegh, Nat. Biotechnol. **24**(6), 703–707 (2006)
H.C. Moeller, M.K. Mian, S. Shrivastava, B.G. Chung, A. Khademhosseini, Biomaterials **29**(6), 752–763 (2008)
J.C. Mohr, J.J. de Pablo, S.P. Palecek, Biomaterials **27**(36), 6032–6042 (2006)
N. Otsu, IEEE Trans. Syst. Man. Cyber. **9**, 62–66 (1979)
J.R. Rettig, A. Folch, Anal. Chem. **77**(17), 5628–5634 (2005)
A. Revzin, R.G. Tompkins, M. Toner, Langmuir **19**, 9855–9862 (2003)
A. Revzin, K. Sekine, A. Sin, R.G. Tompkins, M. Toner, Lab. On. Chip. **5**(1), 30–37 (2005)
Y. Schiffenbauer, A. Israeli. Cell Kinetics Ltd (2007).
Y.S. Schiffenbauer, Y. Kalma, E. Trubniykov, O. Gal-Garber, L. Weisz, A. Halamish, M. Sister, G. Berke, Lab. On. Chip. **9**(20), 2965–2972 (2009)
Y. Shimizu, R. Demars, J. Immunol. **142**(9), 3320–3328 (1989)
A.M. Skelley, O. Kirak, H. Suh, R. Jaenisch, J. Voldman, Nat. Meth. **6** (2), 147–152 (2009)
J.L. Spudich, D.E. Koshland, Nature **262**(5568), 467–471 (1976)
S.S. Stensaas, L.J. Stensaas, Acta Neuropathol. **41**(2), 145–155 (1978)
K.Y. Suh, J. Seong, A. Khademhosseini, P.E. Laibinis, R. Langer, Biomaterials **25**(3), 557–563 (2004)
H.A. Svahn, A. van den Berg, Lab. On. Chip. **7**(5), 544–546 (2007)
W.H. Tan, S. Takeuchi, Proc. Natl. Acad. Sci. U. S. A. **104**(4), 1146–1151 (2007)
R.H. Templer, O. Ces, J. R. Soc. Interface **5**, S111–S112 (2008)
B. Vanherberghen, O. Manneberg, A. Christakou, T. Frisk, M. Ohlin, H.M. Hertz, B. Önfelt, M. Wiklund, Lab. On. Chip. **10**(20), 2727–2732 (2010)
G. Voskerician, M.S. Shive, R.S. Shawgo, H. von Recum, J.M. Anderson, M.J. Cima, R. Langer, Biomaterials **24**(11), 1959–1967 (2003)
S. Yamamura, H. Kishi, Y. Tokimitsu, S. Kondo, R. Honda, S.R. Rao, M. Omori, E. Tamiya, A. Muraguchi, Anal. Chem. **77**(24), 8050–8056 (2005)